Influence of stiffener geometry and anchor bolt loss on the mechanical and fatigue behavior of street lighting poles.

Abstract

Street lighting poles, generally manufactured from galvanized steel, aluminum, or cast iron, play a major role in urban development by ensuring safety, comfort, and aesthetic quality of public spaces. Their dimensioning, particularly at the pole base level, can be performed according to Eurocode 3 - Part 1.8 using the component method. However, these structures are subject to cyclic loading, primarily due to wind, which can generate fatigue phenomena and premature failures, particularly in stress concentration zones such as the pole-base plate junction and anchor rod connections. To improve the resistance of these critical areas, several solutions are commonly considered, including the addition of stiffeners at the pole base and increasing the thickness of the base plate. Nevertheless, the real effectiveness of these measures in terms of fatigue performance requires further investigation.This paper presents a numerical study of the mechanical and fatigue behavior of metallic street lighting pole bases using a three-dimensional model developed in ANSYS Workbench, incorporating all structural components. The results highlight, on the one hand, the influence of the loss of an anchor rod on the structural response of the pole in terms of stress distribution and fatigue life. On the other hand, three stiffener configurationsare analyzed to identify the most effective solution for improving the resistance of pole bases.Among the three configurations analyzed, the third model provides the best compromise, using less material while reducing local stress concentrations and significantly improving the fatigue performance of the structure. Indeed, 28% improvement in fatigue resistance in terms of service life is observed in case 3 compared to case 1.

Keywords: Street lighting poles, Cyclic load,Fatigue life, Stiffeners, Anchor rod loss, AnsysWorkbench

I. Introduction

Street lighting poles (candelabra) play a crucial role in securing and developing urban and road spaces. Their presence ensures satisfactory nighttime visibility for users while also serving as a vital element of the aesthetic design of urban infrastructure [1]. These structures, although relatively simple in appearance, are subject to complex mechanical cyclic loads. These repeated stresses can, over time, induce fatigue phenomena capable of compromising the safety and durability of the structural element. Street lighting poles vary according to several typologies based on diverse criteria such as:

- material : aluminum, stainless steel [2], concrete,

- shape and height[3],
- the implementation method [4],poles embedded directly in concrete foundations, fixed via a welded base plate, etc.

For steel street lighting poles, the most frequently used implementation method consists of welding the pole to a base plate fixed at its end with or without stiffeners. This base plate is then secured in position by anchor rods [5],[6], [7],[8], [9]. The structural arrangement selected for this study concerns tubular poles with circular cross-sections equipped with 4 anchor rods. As illustrated in figure 1 and 2.

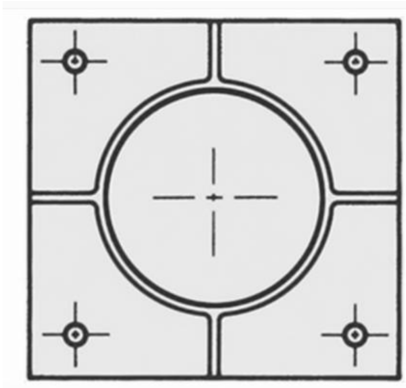

Figure 1: Circular tubular pole

Pole bases continuously experience cyclic loads due to wind action, which induce bending stresses and vortex-induced vibrations particularly pronounced in high masts [10]. Moreover, according to [11], daily and seasonal thermal fluctuations cause repeated metal expansion and contraction, contributing to the evolution of residual stresses and progressive weakening of assemblies by fatigue. Street lighting poles are subjected to time-varying stresses, whether cyclical loads linked to wind action, thermal fluctuations, or environmental vibrations. This dynamic phenomenon, called fatigue [12], [13], causes progressive deterioration of material properties and structural failure even when properly dimensioned under static conditions [14].

In the current context, where the lightweight design of metallic structures has become a major economic priority, the reduction in raw material consumption makes it necessary to account for fatigue phenomena from the design phase to optimize material distribution while ensuring structural reliability and safety. This study does not account for temperature variation or the corrosion effect on stress estimation and fatigue life prediction. Furthermore, wind action is assumed to be variable with constant amplitude.

2. Presentation of the connection and numerical model

Numerical modeling constitutes a particularly relevant tool for analyzing the local and global phenomena to which these structures are subjected, particularly in studying the mechanical behavior of street lighting pole bases.Critical zones, such as the pole-to-base plate junction, welds, or anchorages (Figure 2) present geometric discontinuities and stress concentrations that are difficult to calculate using simplified approaches.

Figure 2: Streetlight pole base

The finite element method allows for realistic representation of the interaction between different components (base plate, pole, stiffeners, anchor rods, concrete foundation) and evaluates the response of the entire system under wind-induced loading. It also provides the possibility of rigorously comparing geometric or constructive variants and measuring their impact on stiffness, stress distribution, and fatigue resistance.

2.1. Numerical modelof the streetlight pole

The structure studied is composed of a tubular metal pole with circular cross-section, fixed to a concrete foundation by a welded base plate and anchor rods. This system is representative of street lighting pole commonly used in urban and road lighting infrastructure. The dimensions and configurations are chosen to faithfully represent assemblies commonly encountered in street lighting infrastructure.

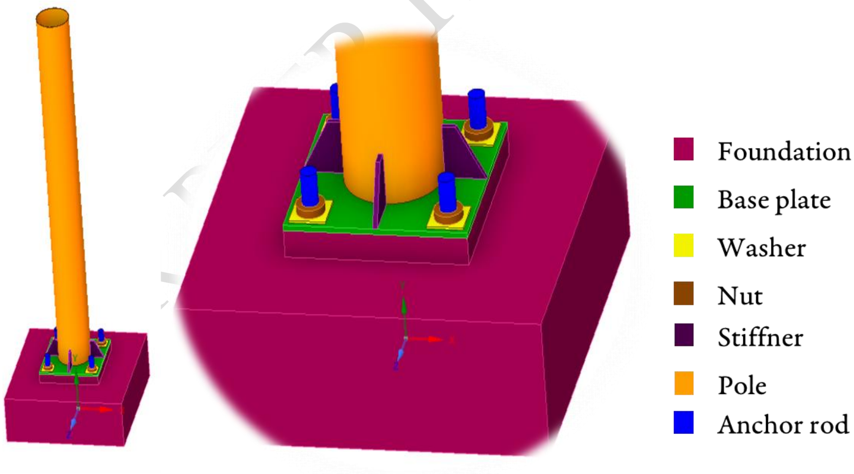

Figure 3: Realistic modeling of the candelabra

In this study, the dimensions are taken from a model of a lighting pole currently located at ÉcolePolytechnique de Thiès(Figures 2).

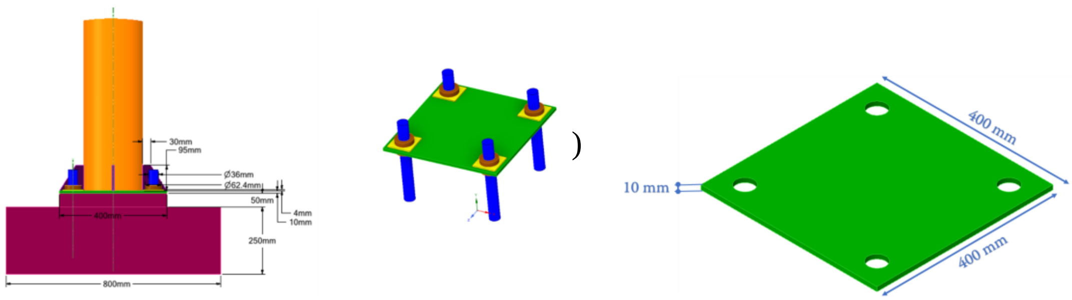

a) b)

Figure 4: a) Dimensions of the pole base, front view of the model, b) Base plate dimensions

A washer measuring 80×80×4 mm ensures proper stress distribution between the base plate and nut to avoid base plate punching. The trapezoidal stiffener contributes to the stiffness of the pole-base plate system (Figure 5).

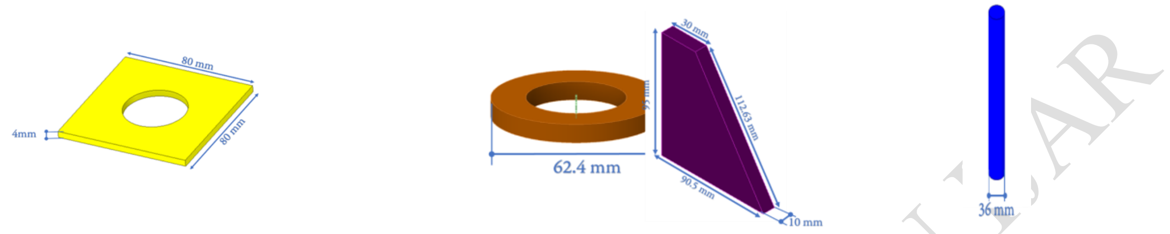

a) washer b) nut c) stiffenerd) anchor rod

Figure 5: Details of the connection at the pole base

2.2. Material mechanical properties

The structure consists of two types of materials: steel and concrete. The properties of these materials used in this study are presented in Tables 1 and 2. The Young's modulus of steel is 200,000 MPa while that of concrete is 30,000 MPa.

Table 1: Mechanical properties of the steel

	A	B	C
1	Propriété	Valeur	Unité
2	Variables des champs matériaux	Tableau	
3	Masse volumique	7850	kg m^-3
4	Coefficient isotrope sécant de dilatation thermique		
5	Coefficient de dilatation thermique	1.2E-05	C^-1
6	Elasticité isotrope		
7	Dériver de	Module ...	
8	Module de Young	2E+05	MPa
9	Coefficient de Poisson	0.3	
10	Module de Compression	1.6667E+11	Pa
11	Module de cisaillement	7.6923E+10	Pa
12	Paramètres de fatigue basée sur les déformations		
20	Courbe S-N	Tabulaire	
21	Interpolation	Semi-log	
22	Echelle	1	
23	Décalage	0	MPa
24	Limite élastique en traction	250	MPa
25	Limite d'élasticité en compression	250	MPa
26	Limite à la rupture en traction	460	MPa
27	Résistance ultime à la compression	0	Pa

Table 2: Mechanical properties of the concrete

	A	B	C
1	Propriété	Valeur	Unité
2	Variables des champs matériaux	Tableau	
3	Masse volumique	2300	kg m^-3
4	Coefficient isotrope sécant de dilatation thermique		
5	Coefficient de dilatation thermique	1.4E-05	C^-1
6	Elasticité isotrope		
7	Dériver de	Module ...	
8	Module de Young	30000	MPa
9	Coefficient de Poisson	0.18	
10	Module de Compression	1.5625E+10	Pa
11	Module de cisaillement	1.2712E+10	Pa
12	Courbe S-N	Tabulaire	
13	Interpolation	Log-log	
14	Echelle	1	
15	Décalage	0	MPa
16	Limite élastique en traction	0	Pa
17	Limite d'élasticité en compression	0	Pa
18	Limite à la rupture en traction	5E+06	Pa
19	Résistance ultime à la compression	4.1E+07	Pa

2.3. Contact Management

The types of contact between parts were defined to reflect as closely as possible the actual functioning of the structure. Thus, frictionless contact is applied between the base plate and the concrete foundation (Figure 6). In this way, the base plate can separate from the concrete foundation. The connection between the base plate and the washer is a rough contact. This means the surfaces are in contact with no sliding allowed in the tangential direction, but separation is allowed in the normal direction. For other contact zones, total connection without part separation is applied (Figure 7).

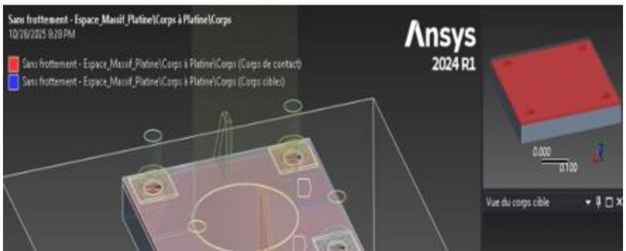

Figure 6: Frictionless contact between the plate and the concrete mass

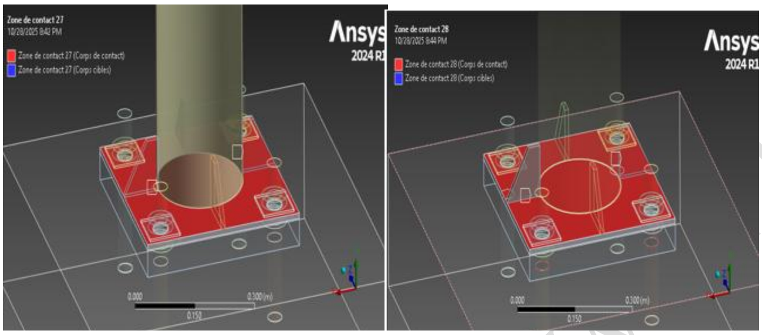

a) **b)**

Figure 7: a) Contact between plate and pole; b) Contact – between stiffener and plate

2.4. Loading and boundary conditions

The street lighting pole is subjected to wind loading. The wind loading is calculatedin accordance with standard NF EN 40-3-1[15], considering aerodynamic and geometric parameters of the pole (Table 3).

$$q_p(y) = \delta \cdot \beta \cdot f \cdot C_e(y) \cdot q(10) \quad \text{(Eq .1)}$$

Where:

- q(10) is the reference wind pressure considering the geographic location of the street lighting pole. The other parameters presented in Equation 1 are defined in the standard [15].

$$q(10) = 0{,}5\rho C_s^2 V_{ref}^2 (N/m^2)$$

- δ is the candelabra size coefficient
- β is the dynamic behavior coefficient of the candelabra
- f is the topography coefficient
- $C_e(y)$ is the terrain- and height-dependent coefficient
- q(10), f and $C_e(y)$ are determined according to ENV 1991-2-4.The heighty of the candelabra is 9 m.

The wind pressure on the street lighting pole (table 3) is illustrated in figure 8.

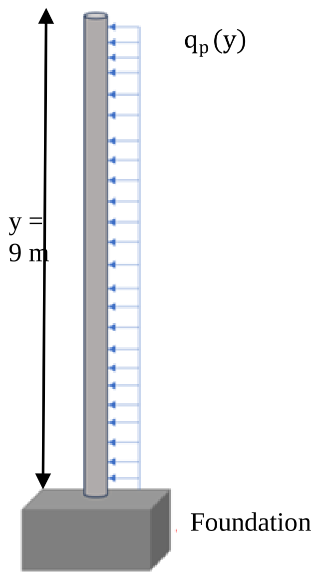

Figure 8: Illustration of the wind pressure on the candelabra

The horizontal component of wind force, F_c, acting on a pole section perpendicular to wind direction is calculated with [15]:

$$F_c = A_c \, c \, q_p(y) \qquad \text{(Eq .2)}$$

- c is the shape coefficient
- A_c is the projected area on a vertical plane perpendicular to the wind direction of the considered section of the shaft

Table 3: Wind Calculation Parameter

Reference velocity (m/s)	V_{ref}	17
Section area (m^2)	A_c	1.971
Reference wind pressure (N/m^2)	q(10)	166.175
Characteristic pressure (N/m^2)	$q_p(y)$	1468.28
Horizontal force on pole shaft (kN)	F_c	**1.6**

The calculated wind pressure was multiplied by the estimated exposure surface of the street lighting pole to obtain a force of approximately 1.6 kN. By simplification and to be conservative, this point load is applied on the upper face of the pole (Figure 9).

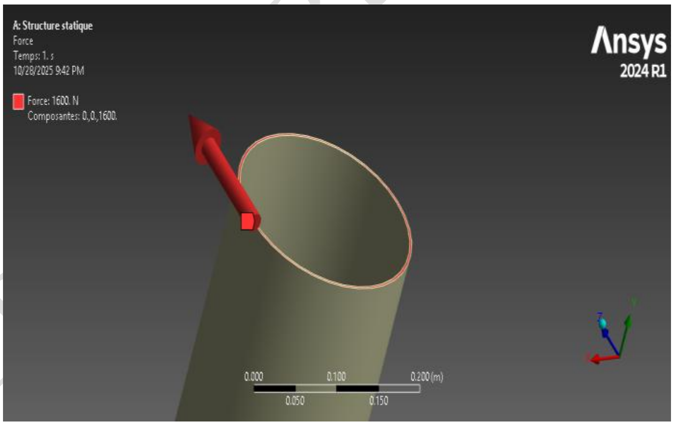

Figure 9: Wind force exerted at the top of the pole

A fixed support is applied to the lower part of the concrete foundation as illustrated in figure 10.

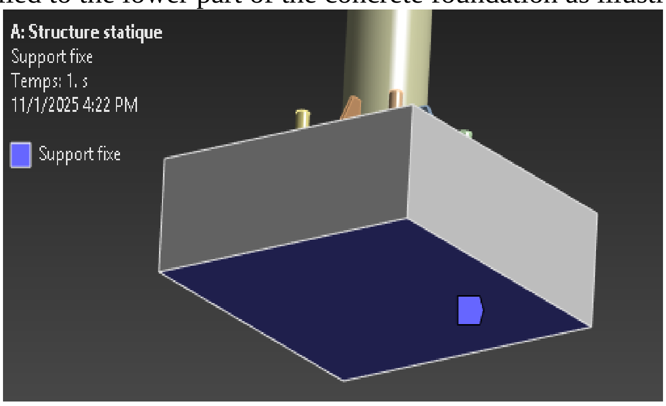

Figure 10: Boundary Condition

2.5. Mesh

Following mesh convergence study and considering machine capabilities and computation time, the mesh sizes given in Table 4 are retained for the study.

Table 4: Mesh size of components

Components	Mesh size (mm)
Foundation	50
Pole	50
Washers	25
Nuts	25
Anchor rods	25
Base plate	25

The meshing result is illustrated in figure 11.

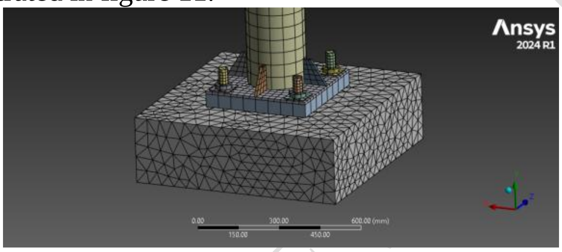

Figure 11: Meshoffinite element model

3. Material fatigue

Fatigue damage is the progressive and irreversible deterioration of a material subjected to cyclic loading (repeated or fluctuating stresses or strains), leading to the initiation and growth of microcracks and potentially resulting in final fracture after a certain number of cycles (fatigue life), even when the applied stress levels are below the material's static strength. It is therefore essential to integrate fatigue analysis from the design stage to ensure the reliability of components. Traditionally, a prototype is created and tested for endurance, but this approach is costly and slow. Nowadays, the goal is to reduce in-service testing by using software tools that allow for rapid simulation of a component's fatigue behavior under random loads.

In service, a mechanical component may be subjected to different operating conditions and, consequently, to several loading sequences, including constant amplitude periodic loading, which is assumption adopted in this study.
Several damage accumulation laws have been proposed in the literature. Some are linear, such as Miner's law, while others, including the model jointly developed by Lemaitre and Chaboche [16], are nonlinear. The majority of damage accumulation laws were reviewed by Fatemi et al. [17] and Shen [18]. These approaches were developed following Palmgren proposal of the linear cumulative damage rule in 1924. However, none of the existing damage accumulation laws can be considered universal, meaning that none can accurately describes all fatigue situations encountered in practice. Nevertheless, in uniaxial fatigue analyses, the law based on Palmgren's linear accumulation, proposed by Miner in 1945, remains the most widely used due to its simplicity and the validity of the results it provides.
According to Miner's rule, for a loading cycle characterized by a mean stress σ_m and a stress amplitude σ_a(figure 12), the material fatigue life N_i corresponding to this cycle can be determined from the Haigh diagram and the S-N curve (figure 13).

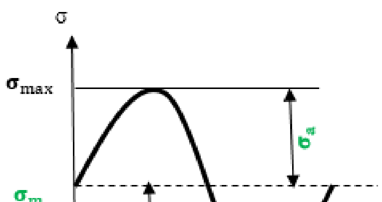

$$\begin{cases} \boldsymbol{\sigma}_{max} = \boldsymbol{\sigma}_m + \boldsymbol{\sigma}_a \\ \boldsymbol{\sigma}_{min} = \boldsymbol{\sigma}_m - \boldsymbol{\sigma}_a \end{cases}$$

Figure 12: Construction of the stress cycle based on its mean value σ_m and its amplitude σ_a

The damage associated with one cycle is expressed as:

$$d_i = \frac{1}{N_i}$$

If the material is subjected to n_i identical cycles, the accumulated damage becomes:

$$D = \sum d_i = \frac{n_i}{N_i}$$

The damage parameter D is dimensionless [19]. It is used to quantify the state of damage progression leading to crack initiation within the material:

- $0 < D < 1$: the material is undamaged after N cycles,
- $D \geq 1$: a crack initiates after N cycles.

This classical uniaxial fatigue life calculation methodology is the one used for damage and fatigue life estimation in this work using ANSYSsoftare. Estimating damage and fatigue life requires, firstly, knowledge of the stress state (equivalent Von Mises stress) at each node of the model (numerical simulation) and, secondly, knowledge of the material's fatigue properties through the S-N curve and the Haigh diagram. Several Haigh diagram models exist in the literature. Examples include the Söderberg model, the Goodman model, the Gerber model, the Morrow model, the DIN model. Experience shows that the Söderberg line and the Goodman line are generally conservative for this loading configuration [20], [21].

Fatigue analysis is performed using ANSYS fatigue module. Wind action is considered as a repeated loading with zero load ratio ($R = 0$ and $\sigma_m > 0$). Furthermore, the mean stress theory based on Goodman's line is adopted for the analysis. By analogy with static analysis of a structure, where care is taken not to exceed the allowable stress, fatigue analysis similarly requires that alternating stress (σ_a) remain below a limit value derived from the S-N curve. This curve expresses material behavior under fatigue in the same manner that elastic stress characterizes static behavior.
Only the steel portion of the structure is analyzed for fatigue. In other words, fatigue analysis does not concern the concrete foundation portion. The S-N curve chosen (Figure 14) and implemented in ANSYS Workbench for steel is that of detail category 40 (Figure 13) given by Eurocode 3 - Part 1.9 [22].

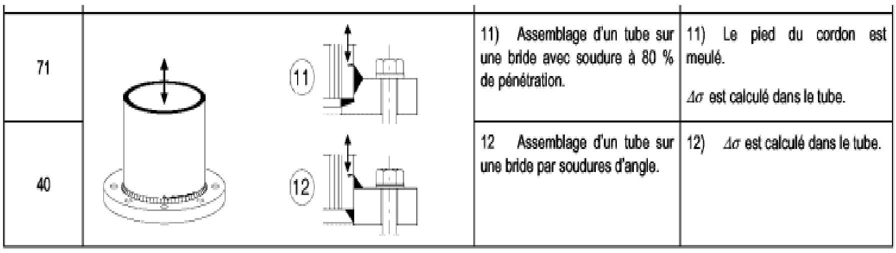

71	(11)	11) Assemblage d'un tube sur une bride avec soudure à 80 % de pénétration.	11) Le pied du cordon est meulé. $\Delta\sigma$ est calculé dans le tube.
40	(12)	12 Assemblage d'un tube sur une bride par soudures d'angle.	12) $\Delta\sigma$ est calculé dans le tube.

Figure 13: Detail category - Eurocode 3 – Part 1.9 [22]

The S-N curve associated with category 40 (Figure 14) is more conservative, as it assumes lower fatigue resistance, justifying this choice.

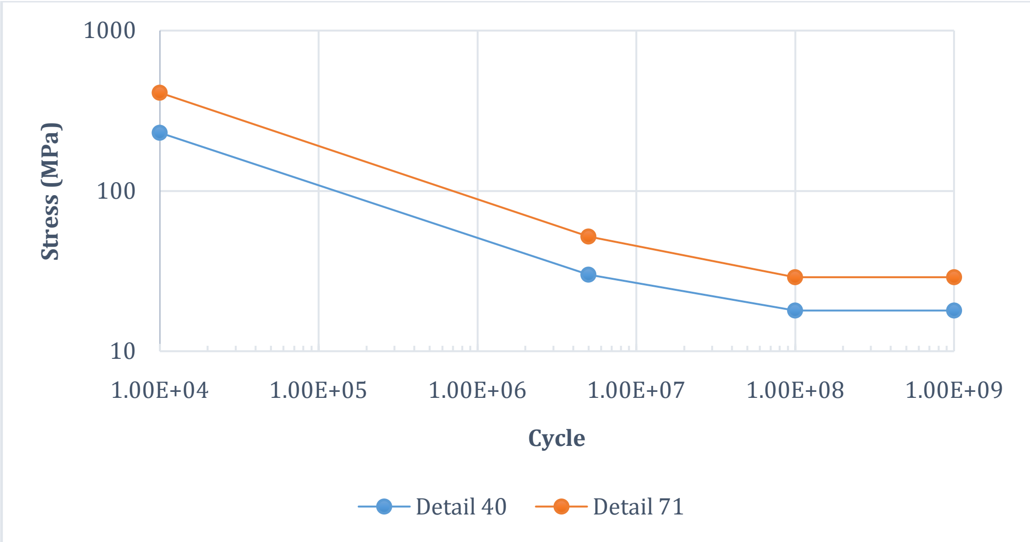

Figure 14: SN curve for steel – Detail categories 40 and 71

4. Results and Discussion

4.1. Influence of the Loss of an Anchor Rod

Anchor rods ensure the transfer of tensile and shear forces between the base plate and the concrete foundation. Their absence, whether due to failure in service, an installation defect, or progressive loosening, can significantly alter the distribution of forces and induce localized stress concentrations. Thus, quantifying the influence of the loss of an anchor rod on the mechanical strength and fatigue resistance of the base of a street lighting pole highlights the importance of prompt maintenance of street lighting pole bases in this situation. For this analysis, two distinct configurations are studied with the same boundary and loading conditions. The only difference between these configurations is the absence of an anchor rod in the second configuration (Figure 15).

- Case 1: tubular pole, 10 mm thick base plate, stiffeners, and four anchor rods.
- Case 2: tubular post, 10 mm thick base plate, stiffeners and three anchor rods.

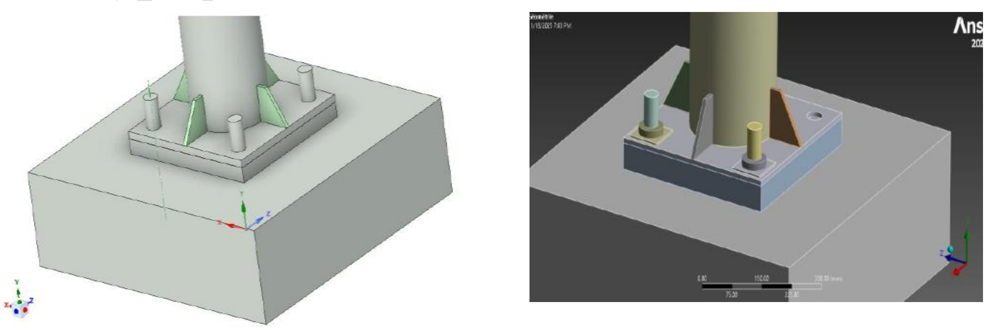

Case 1: 4 anchor rods Case 2: 3 anchor rods

Figure 15: Configurations selected for analyzing the influence of the loss of an anchor rod

This absence of an anchor rod in case 2 simulates a failure or implementation defect scenario, allowing us to study its impact on the distribution of forces, localized stresses, and the fatigue resistance of the structure.

With the same boundary and loading conditions, both configurations lead to the stress distribution illustrated in Figure 16, with a maximum Von Mises equivalent stress of 128.42 MPa in case 1 and 238.8 MPa in case 2.

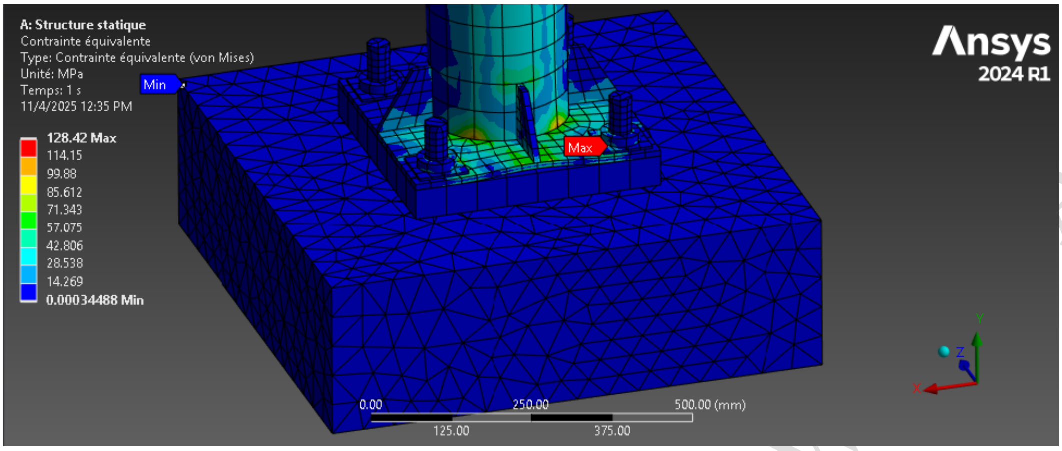

Case 1: 4 anchor rods

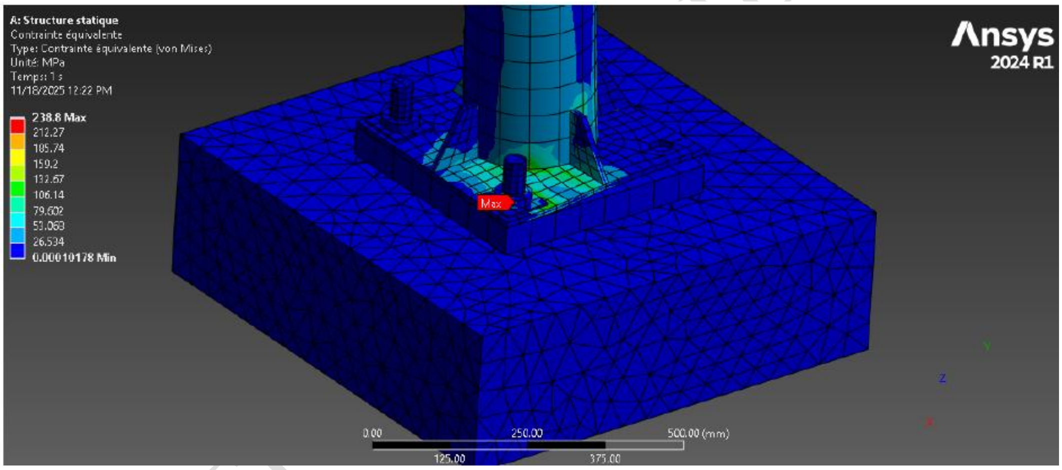

Case 2: 3 anchor rods

Figure 16: Stress mapping

The absence of an anchor rod (case 2) resulted in a stress increase of a factor of 1.86 compared to the reference configuration (case 1). This stress increase in case 2 is explained by a redistribution of stresses on the remaining rods, but also by the detachment of the base plate (Figure 17), which generated a parasitic moment in the anchor rods of configuration 2. Furthermore, a column head displacement (U) twice as large in case 2 compared to case 1 was observed (Table 5).

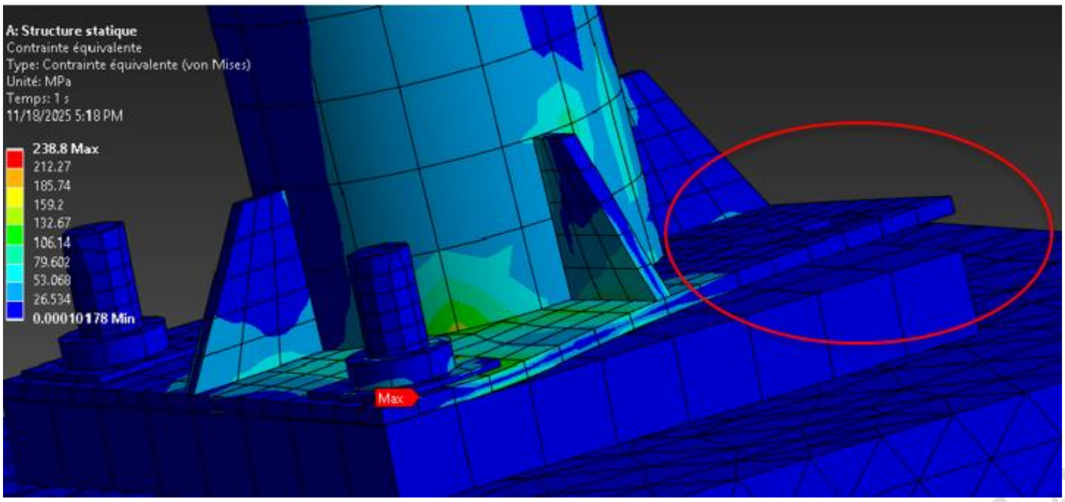

Figure 17: Plate detachment in case 2

The increase in equivalent stress (σ_{VM}) led to a decrease in fatigue life (N_f)), as shown in Table 5.

Table 5: Results of numerical simulations on the influence of anchor rod loss

Case	U (mm)	σ_{VM} (MPa)	N_f(10^4cycles)
1	4.79	128.42	74.8
2	8.90	238.8	1 .87

The fatigue life decreased from 74.8 x 10^4 cycles in case 1 to 1.87 x 10^4 cycles in case 2, representing a reduction of approximately 98%. Analysis shows that the absence of one of the anchor rods leads to a stress increase of nearly 86%. This results in a significant degradation of the fatigue life (table 5).

4.2. Influence of stiffener geometry

In many assemblies, particularly for lighting poles, a small gap is often intentionally introduced between the stiffener and the base plate-column junction (Figures 18b and 18c) to facilitate adjustment, reduce material usage, or simplify manufacturing. This analysis aims to highlight the impact of this material removal at the base of the stiffeners, at the column-base plate intersection, on the structural integrity. Specifically, it seeks to demonstrate through numerical simulation whether this practice is mechanically sound, whether it affects the structure's fatigue resistance, or whether it can, on the contrary, constitute an acceptable or even advantageous solution.

To this end, three models were studied. Model 1 (Figure 18a) represents conventional full-angle stiffeners at the column-base plate junction. In model 2, material was removed from the base of the stiffeners, creating a void beneath them (Figure 18b). The stiffeners remain welded to the column and the base plate, but no longer form the solid right angle of model 1. Finally, model 3 replicates the exact geometry of model 2, but with rounded edges on the column side to eliminate stress concentrations caused by sharp edges.

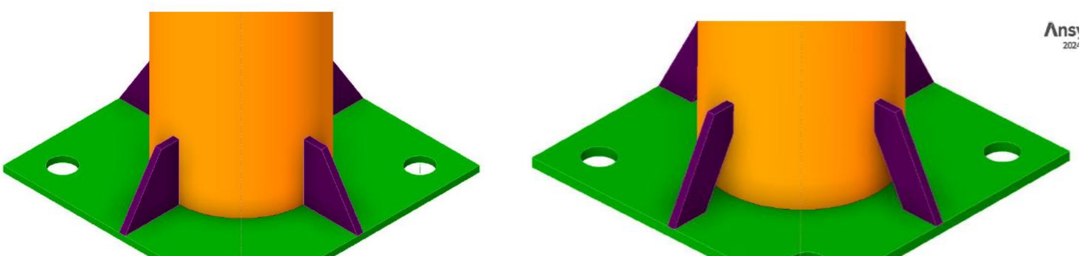

5. Conclusion

a) Model 1 b) Model 2

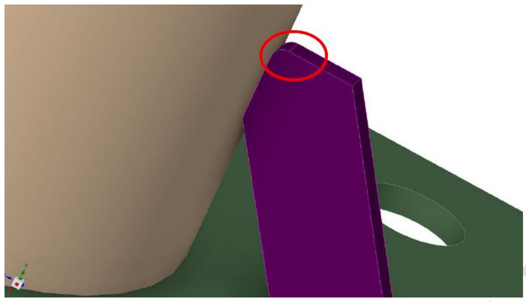

b) Model 3

Figure 18: Analyzedstiffenermodels

Note that the structural geometry, boundary conditions, and loading conditions remain unchanged. Only the stiffener geometry changes in this study.The results obtained for the three configurations are summarized in Table 6.

Table 6: Numerical simulation results for stiffener shapes

Models	U (mm)	σ_{VM} (MPa)	N_f(10^4Cycles)
1	4.79	128.42	74.8
2	4.84	138.24	56.2
3	4.54	119.73	95.7

When switching from model 1 to model 2, the equivalent Von Mises stress increases from 128.42 MPa (Figure 16 - Case 1) to 138.24 MPa (Figure 19a), representing a 7.6% increase in stress. At first glance, this result seems to indicate that material shrinkage could be detrimental. However, a more detailed analysis shows that the maximum stress in model 2 is located precisely at the sharp edge left by the modification (Figure 19b). The increase in stress is therefore not due to material shrinkage itself, but to the presence of this sharp edge, which acts as a notch in the column wall, as evidenced by the results of model 3 (Table 6 and Figure 19c).

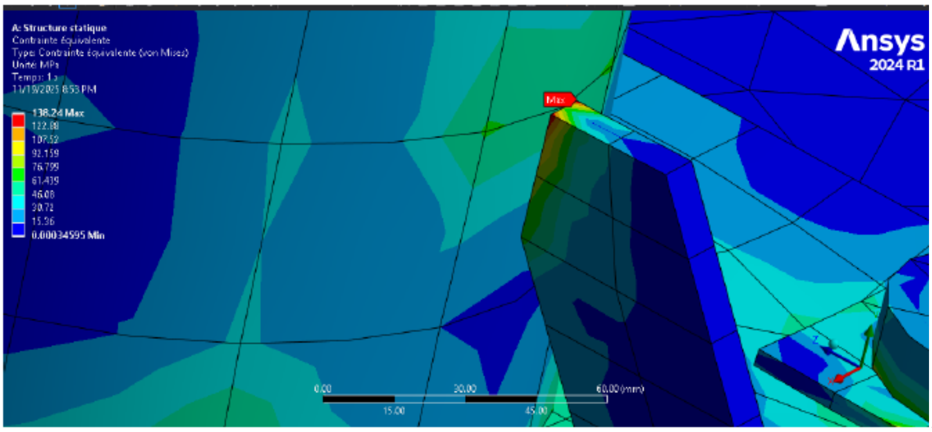

a) Model 2

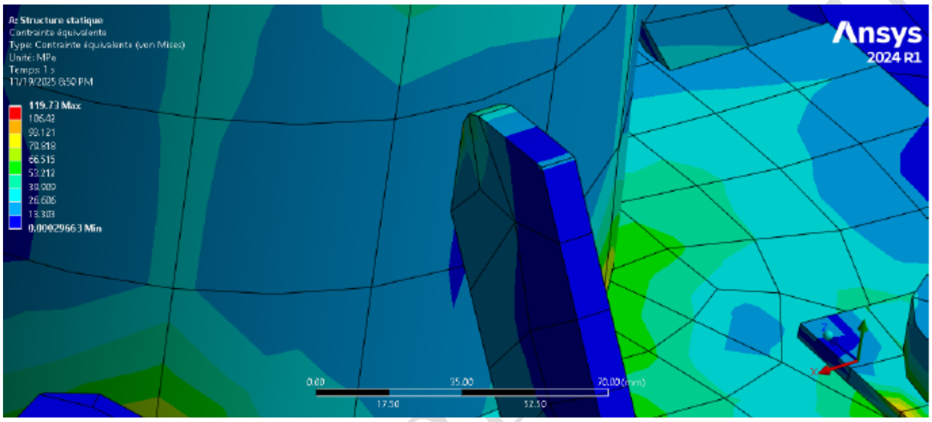

b) Model 3

Figure 19: Stress mapping of different stiffener models analyzed

Rounding the edges (model 3) on the column side reduced the stress concentrations induced by the sharp edges (model 2), decreasing the maximum stress from 138.24 MPa for model 2 to 119.73 MPa for model 3.

Thus, the analysis showed that material removal does not inherently lead to an increase in stress or a degradation of service life, as observed between models 1 and 2. Indeed, the results reveal that the behavior of model 2 was actually biased by the notch effect and did not reflect the true effect of material removal. Once this edge is removed, the configuration becomes not only viable but even more efficient than model 1. Consequently, model 3 results in less displacement at the column top. Indeed, the displacement (U) at the top of the pole decreases from 4.84 mm in model 2 to 4.54 mm in model 3 (Figure 20 and table 6).

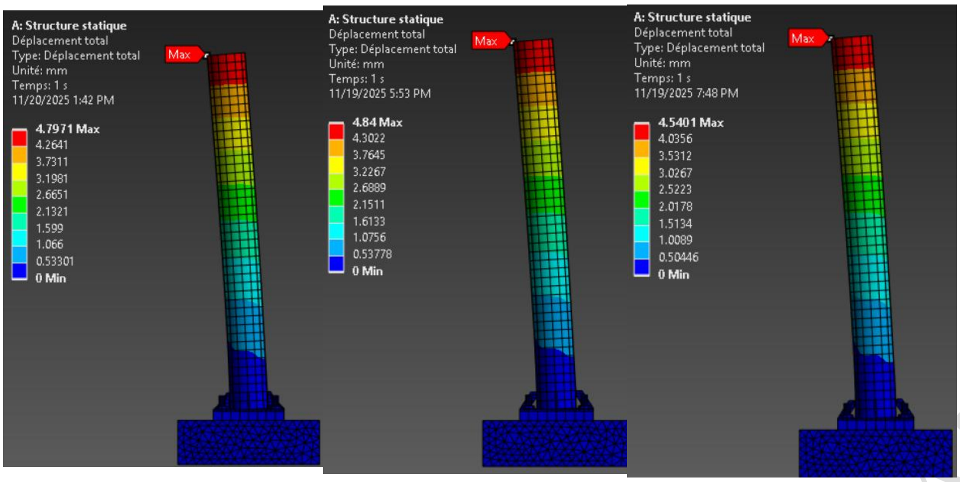

Case 1 Case 2 Case 3

Figure 20: Displacement mapping of different stiffener models analyzed

Furthermore, a stress reduction of nearly 6.8% in model 3 compared to model 1 was observed, increasing the fatigue life from 74.8 × 10^4 cycles to 95.7 × 10^4 cycles, representing a 28% improvement in fatigue resistance in terms of service life. Grinding welds and sharp edges (model 3) is an essential practice for improving the fatigue resistance of welded assemblies. Sharp edges (model 2) act like notches, generating local stress concentrations that promote crack initiation under cyclic loading. According to Jian LU [23],the fatigue resistance is governed by multiple factors including loading type, geometric effects surface condition and residual stresses, highlighting the necessity of global design approach. The geometric discontinuities by grinding or rounding significantly reduces the stress concentration factor, resulting in:

- a reduction in stress peaks near welds,
- an improvement in fatigue life.

This numerical analysis showed that the practice of leaving a void under the stiffeners is perfectly viable. Material removal does not necessarily degrade performance, provided that welds and sharp edges are ground to reduce the influence of stress concentrations. Model 3 offers the best compromise among the three models analyzed: it uses less material, reduces local stress concentrations, and improves the fatigue resistance of the structure.

Conclusion

Public lighting poles are subjected to variable loads, primarily due to wind. These repeated stresses can lead to fatigue failures, compromising the durability and safety of the structures. Adding stiffeners at the base of the poles is a commonly considered solution to enhance their strength, but its actual effectiveness remains to be clarified.Thus, this numerical analysis highlighted the influence of stiffener geometry and the loss of an anchor rod on the mechanical behavior of pole bases under wind-induced loads. The simulation showed that the loss of a single anchor rod resulted in a drastic reduction -nearly 98% -in fatigue life compared to the configuration with all four anchor rods. This result underscores the importance of maintenance in such a scenario.Furthermore, the analysis of the stiffener shape's influence reveals that Model 3 offers the best compromise among the three models analyzed: it uses less material, reduces local stress concentrations, and improves the structure's fatigue resistance.

This study has some limitations. First, the modeling of wind loading is simplified, and second, the triaxiality of stress states is not taken into account. Indeed, the stress state on the structure is multiaxial. Taking this triaxiality into account would require the application of multiaxial fatigue criteria, such as the Dang Van criterion (critical plane approach), the Zenner criterion (integral approach) etc. These aspects are currently being addressed in an ongoing study and will complement and extend the findings presented in this article.

Declaration of Conflicting interest

The authors have nothing to disclose.

Data availability statement

The authors confirm that the data supporting the findings of this study are available within the article. Raw data that support the findings of this study are available from the corresponding author, upon reasonable request.

REFERENCES

[1]T. Gong (2025), *Different types of street lights and their applications*, ZGSM, https://www.zgsm-china.com/blog/different-types-of-street-lights-and-their-applications.html#

[2]Shenchong (2023),*Street Light Pole Production And Types*, https://www.shenchong.com/street-light-pole-production-and-types.html

[3] Phoebus (2025),*Curved shape aluminium street lampe pole light*, https://www.phoebuslight.com/showroom/6m-7m-8m-curved-shape-aluminum-street-lamp-pole-light.html

[4]Lumenevo,*Mât d'éclairage extérieur – Acier galvanisé & Composite*,https://www.lumenevo.be/42-mats-eclairage

[5]M. Couchaux (2021),*Pieds de poteaux*, document de cours, https://fr.scribd.com/document/580631727/CoursCHEC-PiedsPoteaux

[6]Y. Lescouarc'h, (1988), *Les pieds de poteaux encastrés en acier*, Editions CTICM, https://fr.scribd.com/document/719080215/Les-Pieds-de-Poteaux-Encastres-en-Acier-Lescouarch

[7]I. Ryan (2010),*Assemblages des pieds de poteaux en acier: dimensionnement des assemblages de pieds de poteaux métalliques encastrés et articulés*, Guide Eurocode, CSTB https://excerpts.numilog.com/books/9782868914408-extrait.pdf

[8]F. Beckers (2019) ,*Interface entre les structures métalliques et leurs fondations*, Mémoire de Master, Université de Liège, https://matheo.uliege.be/bitstream/2268.2/6762/13/Interface%20entre%20les%20structures%20m%C3%A9talliques%20et%20leurs%20fondations.pdf

[9] Y. Lescouarc'h (1982),*Les pieds de poteaux articulés en acier – Dispositions constructives, méthode de calcul, standardisation*. CTICM

[10] M.Zhang et al. (2023), *Wind-Induced Vibration and Vibration Suppression of High-Mast Light Poles with Spiral Helical Strakes*, Buildings, vol. 13, n° 4, p. 907, doi: 10.3390/buildings13040907.

[11] G. Constantinescu et al. (2013),*TR-612, Wind Loads on Dynamic Message Cabinets and Behavior of Supporting Trusses, Final Report*, https://www.intrans.iastate.edu/wp-content/uploads/2018/03/TR-61220Final20Report.pdf

[12] A.B .Camara (2019), *Analyse du comportement en fatigue d'assemblages boulonnés*, Thèse, Université, Clermont-Auvergne, pp. 1-201.

[13] A. Cardou (2006),*Plasticité, fatigue et rupture des matériaux métalliques modèles mécaniques*, Livre, ISBN: 978-2-921180-93-1

[14] S. Maddox (1991),*Fatigue strength of welded structures*, Book, ISBN: 9781855730137

[15] NF EN 40-3-1(2000),*Candélabres d'éclairage public, Partie 3.1 : Conception et vérification – Spécification pour charges caractéristiques*https://fr.scribd.com/document/541745111/NF-EN-40-3-1

[16] J.L. Chaboche, P.M. Lesne (1988),*A non-linearcontinuous fatigue damage model*, Fatigue & Fracture of Engineering Materials& Structures, pp 1-17, Vol.11.

[17] A. Fatemi, L. Yang (1998), *Cumulative fatigue damage and life prediction theories : a survey of the state of the art for homogeneous materials, International Journal fatigue, pp 9-34, Vol. 20*

[18] S. Chen (2012), *Contribution à l'étude du cumul de dommage en fatigue multiaxiale,* Thèse, Université Lille1- Sciences et Technologies, 181 pages

[19] M. Luki (2018), *Construction métallique-Vérification à la fatigue selon les Eurocodes,* Technique de l'Ingénieur

[20] J. Lu (2002), *Fatigue des alliages ferreux-Définitions et diagrammes*, Technique de l'Ingénieur

[21] A. Brand (1984), *Fatigue des alliages ferreux Approche classique*, Technique de l'Ingénieur

[22] EN 1993-1-9 - Eurocode 3 (2005): Design of steel structures - Part 1-9: Fatigue, European Standard, vol. 33,pp. 1-40.

[23] J. LU (2003), *Fatigue des alliages ferreux – Facteurs d'influence*, Technique de l'ingénieur